DOI: 10.1002/chem.200501364

The Intermediate Frequency Modes of Single- and Double-Walled Carbon Nanotubes: A Raman Spectroscopic and In Situ Raman Spectroelectrochemical Study

Martin Kalbac,*[a, b] Ladislav Kavan,[a] Markéta Zukalová,[a] and Lothar Dunsch[b]

Abstract: The intermediate frequency modes (IFM) of single-walled carbon nanotubes (SWCNTs) and double-walled carbon nanotubes (DWCNTs) were analyzed by Raman spectroscopy and in situ Raman spectroelectrochemistry. The inner and outer tubes of DWCNTs manifested themselves as distinct bands in the IFM region. This confirmed the diameter dependence of IFM frequencies. Furthermore, the analysis of inner tubes of DWCNTs allowed a more-precise assignment of the bands in the IFM region to features intrinsic for carbon nanotubes. Although the inner tubes in DWCNTs are assumed to be structurally perfect, the role of defects on IFM was discussed. The dependence of IFM on electrochemical charging was also studied. In situ spectroelectrochemical data provide a means to distinguish the bands of the outer and inner tubes.

Keywords: carbon nanotubes · electrochemistry · intermediate frequency modes · Raman spectroscopy · spectroelectrochemistry

Introduction

Raman spectroscopy is a frequently used spectroscopic method to investigate single-walled carbon nanotubes (SWCNTs) because of the resonant enhancement of the Raman signal. The main components of the spectra of SWCNTs are the radial-breathing mode (RBM), the tangential-displacement mode (TG), the disorder-induced mode (D), and the high-frequency two-phonon mode (G′). The TG mode is observed in the region of 1450–1600 cm^{-1} and, in the case of metallic tubes, it exhibits pronounced Breit-Wigner-Fano (BWF) broadening. The RBM frequency of isolated (nonbundled) SWCNTs (ω) is inversely proportional to the tube diameter (d) [Eq. (1)]:

$$d = C/\omega \quad (1)$$

in which the constant C is reported to be in the range of 224 to 251 $nm\,cm^{-1}$ (see references [1–3]). The D and G′ modes are observed in all kinds of polycrystalline sp^2 carbon materials, however, their physical origin has been explained only recently in terms of the double-resonance theory.[4–6] The D and G′ modes are observed in the spectral regions of 1250–1450 and 2500–2900 cm^{-1}, respectively. The one-phonon second-order Raman D band appears only if there is a breakdown in translational crystal symmetry, which can be caused by defects in the structure. On the other hand, the two-phonon second-order Raman G′ mode occurs independently of the structural defects.

There are additional bands in the region between 600 and 1100 cm^{-1} in the spectrum of SWCNTs. However, only little attention has been paid to this intermediate frequency mode (IFM) region.[7–9] The intensity of these bands is usually around 100 times lower than the intensity of the TG mode, which makes these studies complicated. The IFM bands exhibit dispersive as well as nondispersive behavior. The nondispersive modes were assigned to first-order features. For example, the mode at 850 cm^{-1} is related to the out-of-plane transverse optical-phonon branch in two-dimensional graphite. The dispersive IFM features exhibit steplike dispersion.[7,9] Such behavior cannot be explained by the usual resonance Raman effect. It is assumed that the dispersive IFM features are related to the combination of two phonons, one optical and one acoustic. The frequency of optical phonon exhibits weak dispersion, whereas the frequency of acoustic

[a] Dr. M. Kalbac, Prof. L. Kavan, Dr. M. Zukalová
J. Heyrovský Institute of Physical Chemistry
Academy of Sciences of the Czech Republic
Dolejškova 3, 18223 Prague 8 (Czech Republic)
Fax: (+42) 28-658-2307
E-mail: kalbac@jh-inst.cas.cz

[b] Dr. M. Kalbac, Prof. L. Dunsch
Leibniz Institute of Solid State and Materials Research
The Group of Electrochemistry and Conducing Polymers
Helmholtzstr. 20, 01069 Dresden (Germany)

phonon exhibits strong dispersion. The dispersion of IFM bands can be described by Equation (2):[7,9]

$$\omega_{\mathrm{IFM}}^{\pm} = \omega_{\mathrm{o}}^{\pm} \pm \nu^{\pm} q \qquad (2)$$

in which $\omega_{\mathrm{IFM}}^{\pm}$ is the frequency of the IFM mode, $\omega_{\mathrm{o}}^{\pm}$ corresponds to the frequency of optical phonon, and $\nu^{\pm}$ is the dispersion of both acoustic and optical phonons. The vector q is the wave vector perpendicular to the nanotube axis. From selection rules, the relationship $q = 4/d_{\mathrm{t}}$ is valid for metallic tubes, and $q = 6/d_{\mathrm{t}}$ is valid for semiconducting tubes, in which d_{t} is the tube diameter. The parameters $\omega_{\mathrm{o}}^{\pm}$ and $\nu^{\pm}$ are specific for a sample with the given diameter distribution.[7,9]

A logical progression in the study of IFM on SWCNTs is the study of double-walled carbon nanotubes (DWCNTs). The DWCNTs can be prepared by catalytic arc discharge,[10,11] chemical-vapor deposition,[12] and by heat treatment of fullerene peapods.[13] This last procedure provides the best quality DWCNTs with narrow distribution of diameters.[13,14] The DWCNTs also exhibit strongly resonant and diameter-selective Raman scattering with specific features of inner and outer tubes.[13–16] The inner tubes in ex-peapods DWCNTs exhibit very narrow Raman lines of the radial-breathing mode (RBM).[13–16] This was previously interpreted as a result of their high structural perfection.[14]

Here, we present a comparative study of IFM bands of SWCNTs and DWCNTs. To the best of our knowledge, this is the first study of the IFM features of DWCNTs. Furthermore, we present novel data obtained by in situ Raman spectroelectrochemistry, which supports our studies of RBM, G and G′ modes, and also improves our understanding of the weak features in the Raman spectra of SWCNTs.

Results and Discussion

The Raman spectra of SWCNTs excited by various laser energies are shown in Figure 1. Several bands that correspond to IFM features were observed in the region of 600 to 1200 cm^{-1}. Each laser excitation energy gives a different IFM band pattern, which is consistent with the recent results of Fantiny et al.[7,9] Both the dispersive and the nondispersive modes were identified in our SWCNT samples. The well-resolved nondispersive modes were found at 860 and 1070 cm^{-1}. The nondispersive mode at around 690 cm^{-1} was present, but its intensity was relatively weak. All nondispersive features exhibited variation in the intensity and line shape upon changes in the laser line. This can be explained by diameter dependence of the position of the IFM features. Within the simplest tight-binding approximation, the energy separation of the i-th singularities ΔE_{ii} is inversely proportional to the tube diameter d [Eq. (3)]:

$$\Delta E_{ii} = (2i\gamma_0 a_{\mathrm{CC}})/d \qquad (3)$$

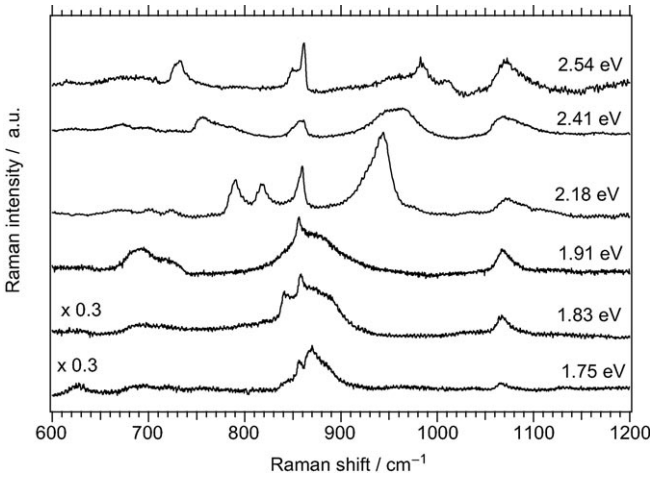

Figure 1. Raman spectra of SWCNTs showing dependence of the bands in the IFM region on laser excitation energy. The laser excitation energy is indicated for each spectrum. Spectra are offset for clarity, but the intensity scale is identical for all spectra, unless stated otherwise.

in which γ_0 is the nearest neighbor overlap integral ($\approx$2.5 eV) and a_{CC} is the C–C bond length ($\approx$142 pm). Due to curvature and many-body effects, the tight-binding model is perturbed, especially for narrow tubes ($d \approx < 1.2$ nm).[17] The change in excitation laser energy leads to selection of SWCNTs in resonance that is dependent on diameter and chirality. As we describe below, the position of IFM bands is diameter dependent in each case. At different excitation energies, tubes with different diameters (and different positions of IFM) are resonantly enhanced, which finally leads to the variation in the shape and intensity of bands. Also, the tubes that do not match the resonant condition perfectly are to some extent resonantly enhanced. This leads also to the relatively broad Raman lines of these features. Furthermore, the intensity of bands is influenced by the relative abundance of resonantly enhanced tubes in the sample at the given laser energy.

The dispersive modes in the Raman spectra of SWCNTs (Figure 1) are well distinguished at the laser excitation energy of 2.54 eV (740 and 950 cm^{-1}), at 2.41 eV (720 and 980 cm^{-1}), and at 2.18 eV (790, 818, and 942 cm^{-1}). On the other hand, they are relatively weak at the laser excitation energies of 1.91, 1.83, and 1.75 eV. Furthermore, it seems that the band with negative dispersion overlaps that of the nondispersive mode at around 860 cm^{-1}. Thus, the previously observed steplike behavior of IFM bands is confirmed.

Figure 2 shows the Raman spectra of DWCNTs excited by the same set of laser energies as those used for the spectra of SWCNTs in Figure 1. The ex-peapod DWCNTs are known to have preferably the diameters of the parent structures, that is, fullerene (C_{70}) and SWCNTs. Because the optimum diameter of a SWCNT for peapod filling is between 1.3 and 1.4 nm,[18] and the optimum interlayer spacing is close to that of the carbon-stacking in graphite (0.34 nm), the diameters of the inner and outer tubes are 0.6–0.9 and 1.3–1.4 nm, respectively.[10,13,14] These two distinct sets of

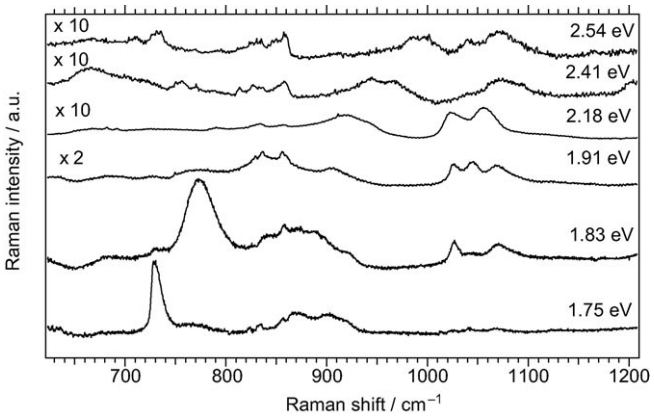

Figure 2. Raman spectra of DWCNs showing dependence of the bands in the IFM region on laser excitation energy. The laser excitation energy is indicated for each spectrum. Spectra are offset for clarity. The intensity of the spectrum excited at 1.91 eV is multiplied by a factor of two, the intensities of the spectra excited at 2.41 and 2.54 eV are multiplied by a factor of ten.

tubes manifest themselves in various Raman features of DWCNTs. The most remarkable feature is observed for RBM, in which two distinct groups of diameters correspond to the bands assignable to outer tubes and inner tubes, respectively. We have also shown previously that the defect-induced D mode and G′ band of DWCNTs exhibit a similar splitting.[15,19] The lower-frequency parts of D or G′ were assigned to inner tubes, and the higher-frequency parts were assigned to outer tubes.

Similar features are observed for IFM bands of SWCNTs and DWCNTs. Generally, the single bands in SWCNTs change to doublets or triplets in DWCNTs spectra. It is assumed that the new bands correspond to IFM features of inner tubes. The shift of the inner-tube band relative to that of the corresponding outer-tube band is dependent on the excitation laser wavelength. In some cases, several IFM bands of inner tubes correspond to one IFM band of an outer tube. For example, at the laser excitation energy of 2.41 eV, the band at 860 cm^{-1} in SWCNTs spectra corresponds to two new bands of inner tubes in DWCNTs spectra at 813 and 828 cm^{-1}. The intensities of IFM of inner tubes in DWCNT spectra vary as the laser excitation energy changes. The signal of inner tubes is much stronger for the 1.75, 1.83, and 1.91 eV laser excitation energies than for the 2.54 or 2.41 eV laser excitation energies. The intensity of the inner-tube bands could be even higher than the intensity of the corresponding outer-tube band, as can be seen for the bands at 784 and 728 cm^{-1} in the spectra excited by 1.83 and 1.75 eV, respectively. The variation in band intensity of IFM of inner tubes in DWCNT spectra can be explained by the different resonance enhancement of inner tubes. The diameter distribution of inner tubes is relatively narrow and most of the inner tubes are resonantly enhanced by the laser energies between 1.7 and 2 eV. Only a small proportion of tubes that might be resonantly enhanced by laser energies of 2.54 or 2.41 eV are present in the ex-peapod DWCNT sample and, therefore, the signal is weak. The bands in DWCNTs, corresponding to the nondispersive IFM features of SWCNTs, were found to be downshifted with respect to the corresponding outer-tube IFM band. The positive correlation of the band position of nondispersive modes with laser excitation is in agreement with theory.[20] The positive correlation with energy is observed also for the D and G′ bands. The frequency dependence of IFM bands is, however, relatively strong and changes as the laser excitation energy changes. The variation in distance between the dispersive IFM of inner and outer tubes observed for different energies could be understood in terms of the model proposed in reference [9]. Tubes with different chiralities and diameters are excited by changing the laser excitation energy. Therefore, different phonons participate in the resonant process as the different E_{ii} and E_{jj} must be connected.[9]

In the case of the 2.18 eV laser excitation, the same number of bands was observed in the region between 750 and 900 cm^{-1} for both SWCNTs and DWCNTs. Furthermore, the band observed at 818 cm^{-1} in the spectra of SWCNTs is upshifted to 833 cm^{-1} in the spectra of DWCNTs. As shown below, the band at 833 cm^{-1} in the DWCNT spectra corresponds to inner tubes. The bands of two dispersive modes of outer tubes are relatively weak, and the one at 818 cm^{-1} can be overlapped with the 833 cm^{-1} band. However, no band of inner tubes that would correspond to the dispersive modes of outer tubes at 790 and 818 cm^{-1} was observed, which indicates the absence of resonant enhancement of dispersive modes for inner tubes.

The appearance of new IFM bands in DWCNT spectra reveals unambiguous and striking features relevant to characterization of carbon nanostructures. The spectra confirm that the IFM bands are diameter dependent. The new bands that appear in DWCNT spectra also verify that the corresponding outer-tube mode is, indeed, attributed to the intrinsic tube modes. The purification process can also modify the tubes. For example, new functional groups can be introduced, whose weak Raman features can be misinterpreted. Therefore, the modes intrinsic for carbon nanotubes have to be determined. The mode at 1050 cm^{-1} was assumed recently to arise from impurity,[9] attributed to C–O–C vibration. On the other hand, we observe two bands in this region for DWCNTs, one corresponding to outer tubes and one to inner tubes. This is in contrast to the mentioned assignment to impurity. The DWCNTs were synthesized at 1200 °C in high vacuum. Such conditions should tend to remove defects rather than to produce them. Furthermore, the inner tubes are formed in the "clean" inner space of SWCNTs. The high quality of inner tubes manifests itself, reportedly, in their narrow RBM bands.[14] Therefore, it is clear that the appearance of a new band as a result of transformation of peapods into DWCNTs must be the intrinsic feature of the carbon nanotube. We assume that this is the case particularly for the 1050 cm^{-1} mode, as the new, slightly downshifted band arises in the DWCNT spectra. This band is assigned to the scattering by the LA phonon around the M point.[21]

Finally, the IFM bands of the inner tubes of DWCNTs are also attributed to rather perfect tubes, as indicated by narrow RBM modes.[22] The role of defects in SWCNTs has been studied recently. The absence of defects contradicts the occurrence of the D mode in the DWCNT spectra, if we assign the low-frequency component of the D band to inner tubes.[16] Therefore, the character of defects in inner tubes must be discussed. The preparation of DWCNTs from peapods is expected to produce relatively short inner tubes. Even if 100% filling is assumed, the amount of carbon available from fullerene as an inner-tube precursor is not sufficient to produce an equally long inner tube inside a particular outer tube. This clearly results in the formation of several short inner tubes within one outer tube. The finite size of tubes is also considered to be a defect. It is apparent that the inner tubes would exhibit more-pronounced finite-size defects. It is difficult to quantify the relationship between the IFM of inner and outer tubes; however, qualitative comparison shows that the IFM of inner tubes are more intense, especially for red lasers. This result supports the assumption that IFM are generated by defects that are associated with the finite length of tubes.

In situ Raman spectroelectrochemistry: Figure 3 shows the dependence on potential of the IFM bands of electrochemically charged SWCNTs. To the best of our knowledge, these bands have not been analyzed by spectroelectrochemistry until now. The bands at 920 and 934 cm^{-1} are assigned to the electrolyte solution and serve as internal standards.

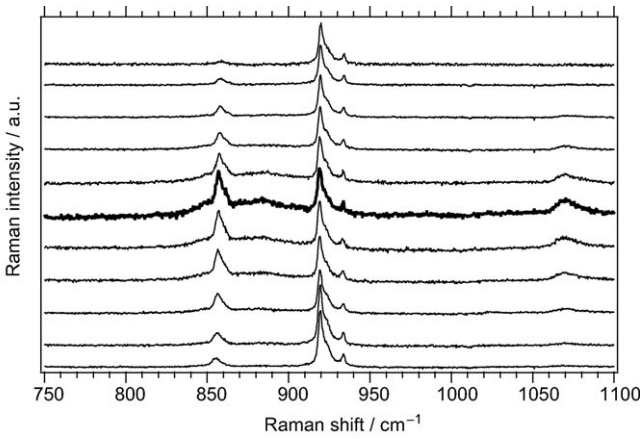

Figure 3. Potential-dependent Raman spectra (excited at 1.91 eV) of SWCNTs on a Pt electrode in 0.2 M $LiClO_4$+acetonitrile. The electrode potential varied by increments of 0.3 V from 1.2 to −1.8 V vs. Fc/Fc^+ for curves from top to bottom. Spectra are offset for clarity, but the intensity scale is identical for all spectra. The peaks at 920 and 934 cm^{-1} are assigned to the electrolyte solution. The bold curve indicates the spectrum of SWCNTs in the nearly undoped state.

Electrochemical charging, both cathodic and anodic, causes the bleaching of both RBM and TG modes of SWCNTs. The change in electrochemical potential leads to a shift of the Fermi level. As the energy of van Hove singularities is achieved, the corresponding interband transition is bleached and the Raman resonance is quenched. This model may, however, oversimplify the situation in spectroelectrochemistry. In fact, the complete quenching of transitions between the first singularities in metallic tubes, E_{11}^{M}, and the second and third singularities in semiconducting tubes, E_{22}^{S} and E_{33}^{S} (which play a role for lasers between 2.54 and 1.91 eV), would require Fermi-level shifts as large as 1 to 1.3 eV. Such shifts are hardly accessible electrochemically, if we take into account that electrochemical double-layer charging typically creates around 0.005 e^-(holes) per carbon atom per volt,[23,24] which translates into the corresponding E_F shifts of approximately 0.3 to 0.6 eV only.[25] Complex relations between the Fermi-level shift and the applied electrochemical potential were recently addressed by Rafailov et al. for metallic tubes,[25] however, a full understanding of the intensity/potential profiles in Raman spectroelectrochemistry still requires further study.

A second distinct effect is the blue-shift of TG of outer tubes upon anodic charging. This is explained by hardening of the C−C bond during anodic charging (p-doping). The attenuation of Raman spectra (excited at 1.91 eV) is usually explained by the loss of resonance through quenching of optical transitions E_{11}^{M} and E_{22}^{S} in narrower tubes. Consequently, the charging also erases the Fano broadening in metallic tubes at both cathodic and anodic potentials.[15] The blue-shift of TG upon anodic charging reflects the stiffening of the graphene mode if holes are introduced into the π band.[26,26] The behavior of the D and G′ modes during electrochemical charging is similar. Both modes are shifted and bleached as the applied charge increases.[15,16] On the other hand, the RBM bands exhibit only bleaching without distinct frequency shifts. This indicates that the position of modes connected to LO phonons are only slightly affected by doping.

The drop in intensity of the IFM band at 857 cm^{-1} shown in Figure 3 is monotonous and almost symmetrical to the maximum intensity observed at the nearly undoped state (bold curve in Figure 3). The small asymmetry in bleaching during the anodic and cathodic doping can be caused by the initial position of Fermi level in carbon nanotubes. The band becomes barely detectable at large cathodic and anodic potentials. This behavior is characteristic for resonant Raman modes of SWCNTs,[26] and confirms that the 857 cm^{-1} mode is intrinsic to tubes and is resonant. The electrochemical doping also leads to the upshift of the IFM at 857 cm^{-1} during the anodic doping. However, the upshift is very small, only 1 cm^{-1} upon progression from +0.3 to +1.8 V vs Fc/Fc^+ (Fc = ferrocene). During cathodic doping, the downshift of about 2 cm^{-1} was observed if the potential is changed from +0.3 to −1.2 V vs Fc/Fc^+. The shift is much smaller than that observed for the TG mode, for which shifts of 10 to 15 cm^{-1} were found (data not shown). Furthermore, during cathodic doping, the upshift of the TG mode was observed, which is contrary to the downshift in the case of the 857 cm^{-1} IFM. The shift of the D mode is also stronger, however, the difference is not so large. The D

mode shifts by about 3 and 8 cm^{-1} during the cathodic and anodic doping, respectively. The direction of shift is the same as for the IFM band.

The band at 1070 cm^{-1} is less intense and it is almost completely bleached at potentials of +1.5 or −0.9 V vs Fc/Fc^+. Due to the fast bleaching of the mode, it is difficult to determine whether the mode shifts or not during electrochemical charging. Finally, the doping-induced bleaching of the band at 1070 cm^{-1} further confirms its assignment to the intrinsic mode of SWCNTs.

Figures 4 and 5 show the dependence on potential of the IFM bands in electrochemically charged DWCNTs. In general, as the electrochemical potential increases, the IFM bands are bleached. This behavior is similar to the behavior of SWCNTs during electrochemical charging. However, it is clear that the bleaching does not occur to the same extent for all bands. The IFM bands assigned to outer tubes exhibit more-pronounced bleaching than the IFM bands assigned to inner tubes, which is a general effect in DWCNTs. As was already shown,[15] the RBMs of inner tubes in DWCNTs are extinguished less than the bands of outer tubes during the application of electrochemical potential. In other words, the inner tubes are shielded by outer tubes, but at high potentials even inner tubes are affected to some extent. A similar effect is observed for chemical p-doping. In this case a three-layer-capacitor model was applied, and it was concluded that most of the holes are located on the outer tube.[27] The hole concentration on outer tubes was found to be approximately ten times higher than in the case of inner tubes. This explains the sluggish intensity attenuation of inner-tube bands. The same conclusion was drawn also for electrochemical doping.[16] Hence, during electrochemical doping, the charge is located preferably on the outer tube, the van Hove singularities of inner tubes are filled at higher potentials, and the inner-tube IFM bands start to bleach at larger potentials. Therefore, postponed bleaching of the bands could be used as an indication of inner-tube features.

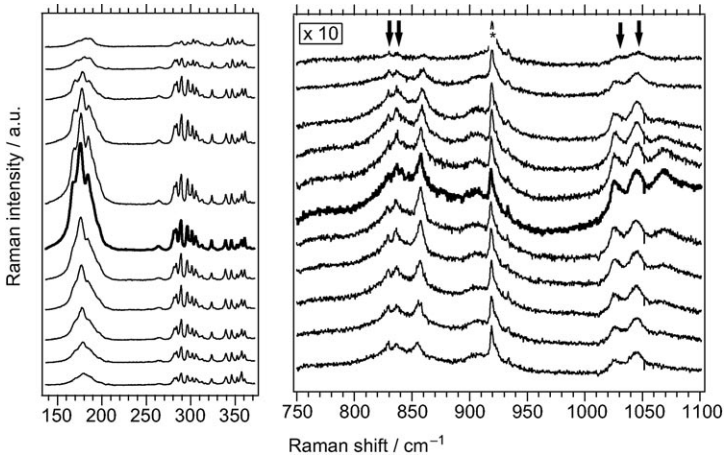

Figure 4. Potential-dependent Raman spectra (excited at 1.91 eV) of DWCNTs on a Pt electrode in 0.2 M $LiClO_4$+acetonitrile. The electrode potential varied by increments of 0.3 V from 1.2 to −1.8 V vs Fc/Fc^+ for curves from top to bottom. Spectra are offset for clarity, but the intensity scale is identical for all spectra. The peaks at 920 and 934 cm^{-1} (marked with *) are assigned to the electrolyte solution. The bands assigned to inner tubes are marked with arrows. The bold curve indicates the spectrum of DWCNTs in the nearly undoped state.

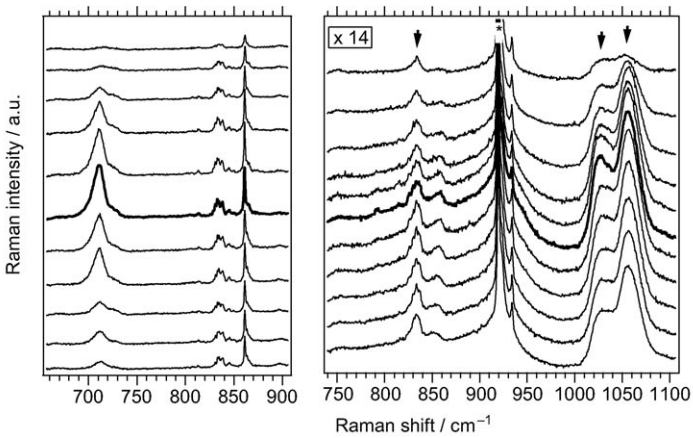

Figure 5. Potential-dependent Raman spectra (excited at 2.18 eV) of DWCNTs on a Pt electrode in 0.2 M $LiClO_4$+acetonitrile. The electrode potential varied by increments of 0.3 V from 1.2 to −1.8 V vs. Fc/Fc^+ for curves from top to bottom. Spectra are offset for clarity, but the intensity scale is identical for all spectra. The peaks at 920 and 934 cm^{-1} (marked with *) are assigned to the electrolyte solution. The bands assigned to inner tubes are marked with arrows. The bold curve indicates the spectrum of DWCNTs in the nearly undoped state.

The spectra of DWCNTs excited by 1.91 eV laser energy exhibit two bands at around 830 and 835 cm^{-1}, which correspond to the outer-tube band at 857 cm^{-1} (Figure 4). The band at 835 cm^{-1} bleaches faster than the band at 830 cm^{-1}. Similarly, the inner-tube modes at 1025 and 1045 cm^{-1} can be related to the outer-tube mode at 1070 cm^{-1}. Again, the different sensitivity to doping-induced attenuation is clearly expressed in Figure 4. The IFM of inner tubes seem to differ in their sensitivity to bleaching. However, these bands are relatively broad and the bleaching occurs only at high potentials, therefore, it is difficult to detect the difference in the bleaching sensitivity of the bands. An analogous effect was observed previously for RBM of inner tubes, which also bleach to different extents.[15,16] The origin of this effect is still not clear. In the case of IFM bands, the speed of bleaching is related to the diameter of the tubes. The band at higher frequency that corresponds presumably to thicker inner tubes bleaches faster. The energy of optical transition E_{ii} decreases as the tube diameter increases [Eq. (2)]. Therefore, for thicker tubes, the filling/depleting of van Hove singularities occurs at lower potentials than for thin tubes. As the availability of optical transition is crucial for the resonance Raman effect, the bands of thick tubes should bleach faster. However, one could argue that only tubes with a suitable band-gap are resonantly enhanced and, thus, observed. In other words, the band-gap of the tubes measured should not differ significantly. However, the resonance condition is not very sharp, and tubes that are not in perfect resonance are seen in the spectra, although with smaller intensity. In

the filling of van Hove singularities, the change in intensity is, therefore, not so pronounced. Thus, the thicker inner tubes are not in perfect resonance, which results in a reduced effect of potential on the change in intensity. The smaller doping sensitivity of tubes that are not in perfect resonance was demonstrated recently by the Raman spectroelectrochemistry of chirality-resolved SWCNTs.[28]

Figure 5 shows the sequence of spectra of electrochemically doped DWCNTs at 2.18 eV excitation. The spectroelectrochemical identification of the bands is very important, as it is difficult to distinguish which bands correspond to the outer and inner tubes, respectively. For example, the band at 833 cm^{-1} could be assigned to the shifted outer-tube dispersive mode or to the inner-tube band that corresponds to the nondispersive outer-tube band at 858 cm^{-1}. The bleaching of the band is suppressed, hence we assigned this band to the inner-tube mode. A similar effect was seen for the double band at 1070 cm^{-1}, which also exhibits weak bleaching and is, therefore, assigned to inner-tube features. The dispersive mode at around 920 cm^{-1} interferes with the bands of acetonitrile, which precludes analysis of its charge-dependent bleaching.

Conclusions

The intermediate frequency mode (IFM) bands in Raman spectra of SWCNTs and DWCNTs were studied. The spectra of DWCNTs exhibited new features in the IFM region, and these were attributed to inner tubes. Comparison of the spectra of SWCNTs and DWCNTs (the latter prepared from peapods) yields the following conclusions:

1) Intrinsic vibrational modes of carbon nanotubes can be identified.
2) The IFM bands are strongly diameter dependent.
3) The IFM bands are, presumably, related to finite-size defects of tubes.

Results of in situ Raman spectroelectrochemistry demonstrated that the delayed bleaching of inner tubes in DWCNTs applies also for the IFM bands of inner tubes. The frequency shift of IFM bands during electrochemical charging is similar to the shift of the D mode, considering the sign and size of the shift. Inner- and outer-tube bands exhibit different sensitivity to electrochemical doping. This effect was used successfully to assign bands to inner and outer tubes. The bleaching of the inner-tube IFM modes was found to be dependent on the inner-tube diameter.

Experimental Section

Single-walled carbon nanotubes (SWCNTs) were available from our earlier work.[24] Double-walled carbon nanotubes (DWCNTs) were prepared by heat conversion of the C_{70}@SWCNT (filling ratio 72%) peapods, which were also available from our earlier work. The conversion of peapods was carried out at 1200 °C in a vacuum for 12 h. The electrodes for in situ spectroelectrochemical studies were fabricated by evaporation of a sonicated ethanolic slurry of SWCNTs on Pt electrodes. The film was outgased at 80 °C in vacuum and then fixed in the Raman spectroelectrochemical cell. The spectroelectrochemical cell was air-tight, had one compartment, and was equipped with a glass optical window for spectroscopic measurements.

The cell was assembled in a glove box (M. Braun); the box atmosphere was N_2, containing O_2 and H_2O each at <1 ppm. Electrochemical experiments were carried out by using PG 300 (HEKA) or 273A (EG&G PAR) potentiostats with Pt-auxiliary and Ag-wire pseudoreference electrodes, the electrolyte solution was 0.2 M $LiClO_4$+acetonitrile (both from Aldrich; the latter dried by using 4 Å molecular sieve). After each spectroelectrochemical measurement, ferrocene (Fc) was added to the cell as a reference for cyclic voltammetry analysis. The potentials related to the Ag pseudoreference were recalculated and referred to the potential of the Fc/Fc^+ electrode.

The Raman spectra were excited by Ar^+ and Kr^+ lasers (Innova 300 series, Coherent), and by a Ti-sapphire laser (899 LC, Coherent). Spectra were recorded by using a T-64000 spectrometer (Instruments SA) interfaced to an Olympus BH2 microscope (objective 50×). The laser power impinging on the cell window or on the dry sample was between 1 and 5 mW. The spectrometer was calibrated by using the F_{1g} mode of Si at 520.2 cm^{-1}.

Acknowledgements

This work was supported by the Academy of Sciences of the Czech Republic (contract no. A4040306) and by the Czech Ministry of Education, Youth and Sports (contract no. LC-510). M. Kalbac acknowledges a grant from the Alexander von Humboldt Foundation.

[1] S. Bandow, M. Takizawa, H. Kato, T. Okazaki, H. Shinohara, S. Iijima, *Chem. Phys. Lett.* **2001**, *347*, 23–28.
[2] T. Pichler, H. Kuzmany, H. Kataura, Y. Achiba, *Phys. Rev. Lett.* **2001**, *87*, 267401.
[3] A. Jorio, R. Saito, J. H. Hafner, C. M. Lieber, M. Hunter, T. McClure, G. Dresselhaus, M. S. Dresselhaus, *Phys. Rev. Lett.* **2001**, *86*, 1118–1121.
[4] J. Kurti, V. Zolyomi, A. Gruneis, H. Kuzmany, *Phys. Rev. B* **2002**, *65*, 165433.
[5] C. Thomsen, S. Reich, *Phys. Rev. Lett.* **2000**, *85*, 5214–5217.
[6] R. Saito, A. Jorio, A. G. Souza, G. Dresselhaus, M. S. Dresselhaus, M. A. Pimenta, *Phys. Rev. Lett.* **2002**, *88*, 027401.
[7] C. Fantini, A. Jorio, M. Souza, L. O. Ladeira, A. G. Souza, R. Saito, G. G. Samsonidze, G. Dresselhaus, M. S. Dresselhaus, M. A. Pimenta, *Phys. Rev. Lett.* **2004**, *93*, 087401.
[8] L. Alvarez, A. Righi, S. Rols, E. Anglaret, J. L. Sauvajol, *Chem. Phys. Lett.* **2000**, *320*, 441–447.
[9] C. Fantini, A. Jorio, M. Souza, R. Saito, G. G. Samsonidze, M. S. Dresselhaus, M. A. Pimenta, *Phys. Rev. B* **2005**, *72*, 085446.
[10] M. Kociak, K. Suenaga, K. Hirahara, Y. Saito, T. Nakahira, S. Iijima, *Phys. Rev. Lett.* **2002**, *89*, 155501.
[11] T. Sugai, H. Yoshida, T. Shimada, T. Okazaki, H. Shinohara, *Nano Lett.* **2003**, *3*, 769–773.
[12] J. Q. Wei, B. Jiang, X. F. Zhang, H. W. Zhu, D. H. Wu, *Chem. Phys. Lett.* **2003**, *376*, 753–757.
[13] S. Bandow, M. Takizawa, K. Hirahara, M. Yudasaka, S. Iijima, *Chem. Phys. Lett.* **2001**, *337*, 48–54.
[14] R. Pfeiffer, H. Kuzmany, C. Kramberger, C. Schaman, T. Pichler, H. Kataura, Y. Achiba, J. Kurti, V. Zolyomi, *Phys. Rev. Lett.* **2003**, *90*, 225501.
[15] L. Kavan, M. Kalbac, M. Zukalova, M. Krause, L. Dunsch, *ChemPhysChem* **2004**, *5*, 274–277.

[16] M. Kalbac, L. Kavan, M. Zukalova, L. Dunsch, *Adv. Funct. Mater.* **2005**, *15*, 418–426.
[17] A. Jorio, C. Fantini, M. A. Pimenta, R. B. Capaz, G. G. Samsonidze, G. Dresselhaus, M. S. Dresselhaus, J. Jiang, N. Kobayashi, A. Gruneis, R. Saito, *Phys. Rev. B* **2005**, *71*, 075401.
[18] S. Okada, S. Saito, A. Oshiyama, *Phys. Rev. Lett.* **2001**, *86*, 3835–3838.
[19] M. Kalbac, L. Kavan, M. Zukalova, L. Dunsch, *Carbon* **2004**, *42*, 2515–2920.
[20] O. Dubay, G. Kresse, *Phys. Rev. B* **2003**, *79*, 035401.
[21] A. Gruneis, R. Saito, T. Kimura, L. G. Cancado, M. A. Pimenta, A. Jorio, A. G. Souza, G. Dresselhaus, M. S. Dresselhaus, *Phys. Rev. B* **2002**, *65*, 155405.
[22] R. Pfeiffer, H. Kuzmany, C. Kramberger, C. Schaman, T. Pichler, H. Kataura, Y. Achiba, J. Kürti, V. Zolyomi, *Phys. Rev. Lett.* **2003**, *90*, 225501.
[23] L. Kavan, L. Dunsch, H. Kataura, *Chem. Phys. Lett.* **2002**, *361*, 79–85.
[24] L. Kavan, L. Dunsch, H. Kataura, A. Oshiyama, M. Otani, S. Okada, *J. Phys. Chem. B* **2003**, *107*, 7666–7675.
[25] P. M. Rafailov, J. Maultzsch, C. Thomsen, H. Kataura, *Phys. Rev. B* **2005**, *72*, 045411.
[26] P. Corio, P. S. Santos, V. W. Brar, G. G. Samsonidze, S. G. Chou, M. S. Dresselhaus, *Chem. Phys. Lett.* **2003**, *370*, 675–682.
[27] G. G. Chen, S. Bandow, E. R. Margine, C. Nisoli, A. N. Kolmogorov, V. H. Crespi, R. Gupta, G. U. Sumanasekera, S. Iijima, P. C. Eklund, *Phys. Rev. Lett.* **2003**, *90*, 257403.
[28] L. Kavan, M. Kalbac, M. Zukalova, L. Dunsch, *J. Phys. Chem. B* **2005**, *109*, 19613–19619.

Received: November 2, 2005
Published online: March 22, 2006

